Formation of two kinds of nonspherical lithium colloids in electron-irradiated Li_2O single crystals

F. Beuneu,* P. Vajda,† and G. Jaskierowicz
Laboratoire des Solides Irradiés, CNRS-CEA, École Polytechnique, F-91128 Palaiseau, France

M. Lafleurielle
Laboratoire de Chimie des Solides, Université Paris-Sud, F-91400 Orsay, France
(Received 15 October 1996; revised manuscript received 26 November 1996)

The two kinds of lithium metal colloids created in single crystals of lithium oxide by electron irradiation near 0 °C manifesting themselves as two electron paramagnetic resonance metallic lines [see F. Beuneu and P. Vajda, Phys. Rev. Lett. **76**, 4544 (1996)] are investigated as a function of impinging electron fluence and after an isochronal annealing treatment. The small ($<1\mu$m) colloids, responsible for the narrow Lorentzian line, anneal near 300 °C, while the large ($\gg 1\mu$m) colloids, giving rise to the Dysonian signal, recover above 400 °C. Dielectric-constant measurements in the microwave frequency range reveal a substantial increase of both real and imaginary parts of ϵ, corroborating the metal colloid formation. An effective medium analysis of the ϵ variation after irradiation suggests nonspherical shapes for the metal colloids. The recovery of the irradiation-induced ϵ increase occurs in the same range as that of the colloid lines, with a peak of $\Delta\epsilon''$ near 400 °C, probably indicating a colloid shape redistribution before decomposition. Finally, electron and optical microscopy results are presented, confirming the existence of two sizes of nonspherical, anisotropically distributed lithium colloids. [S0163-1829(97)06217-6]

I. INTRODUCTION

Among the various ionic crystals which can give rise to intrinsic metal colloid formation,[1] lithium compounds are particularly attractive and were quite extensively studied in the past. Lithium metal precipitation under irradiation with various projectiles occurs easily in these crystals, whereas metal detection can be done by conduction electron spin resonance (CESR), because lithium, the lightest metal known, has virtualy no spin-orbit interaction[2] and so gives very narrow and characteristic CESR signals. Moreover, lithium compounds are intensively studied as prospective first-wall cladding material in fusion reactors, due to the tritium breeding properties of the lithium nucleus, and as battery material because of the high ionic mobility of Li. Finally, lithium oxide (Li_2O) is a choice system for first-principles studies, due to its simple electronic (no *d* electrons) and crystallographic (antifluorite) structure, enabling, for example, *ab initio* calculations of excited electronic states.[3]

We have therefore begun to study Li_2O under irradiation with electrons in the MeV energy range. In our first paper,[4] we reviewed the literature on lithium colloid creation by irradiation of lithium compounds, and an extensive reference list can be found there. As a brief summary we just mention here, for LiF, the work of the Orsay group[5] and, for Li_2O, the work of Noda and his collaborators.[6] Our Ref. 4 was devoted to irradiation of polycrystalline samples of Li_2O with 1 MeV electrons at different temperatures T_{irr} in the range 21 to 275 K. The created defects manifested a strong T_{irr} dependence: (i) At low temperatures, $T_{irr}<200$ K, mainly F^+ centers (O vacancies with a trapped electron) are formed; thermal annealing leads to their recovery near $T_{ann}=400$ °C, which is accompanied by the emergence of a new signal near $g=2.003$, possibly due to their agglomeration into small F^+ clusters. The latter disappear at 600–700 °C. (ii) After $T_{irr}=200$ K, the F^+ spectra are superimposed by the $g=2.003$ line and by a new, narrow signal at $g=2.0023$, caused by small metallic colloids. (iii) At $T_{irr}=275$ K, finally, only a narrow *T*-independent line ($\Delta H\sim 10^{-2}$ mT) is observed at $g=2.00235(2)$, characteristic for metallic Li colloids. The microwave dielectric constant ϵ measured on the same specimens, increased notably after the room-temperature irradiation, emphasizing the presence of metallic particles, while remaining unchanged for lower T_{irr}. Both the colloid line and the radiation-induced $\Delta\epsilon$ vanish simultaneously above $T_{ann}\approx 250$ °C.

It seemed important to irradiate single crystals in order to check for possible anisotropy and also for any difference in colloid growth behavior: preliminary results were given in two recent papers,[7,8] including first NMR observations on the metallic character of the precipitates. There, we had signaled the emergence of two electron paramagnetic resonance (EPR) signals related both to metallic lithium: one narrow Lorentzian line due to small clusters similar to those found in polycrystals,[4] the other a superimposed Dysonian line corresponding to much bigger colloids, typically in the micrometer range. This was in contrast to earlier work on neutron-irradiated LiF (Ref. 5), where the reported two- and three-dimensional clusters were all of much smaller size. In this paper, we present new complementary investigations to these results. After an experimental section (Sec. II), we describe the temperature and the dose dependence of the observed EPR lines (Sec. III), including their behavior with annealing; in Sec. IV are discussed the microwave dielectric constant

measurements; in Sec. V, we present the results of direct observations in both optical and electron microscopy.

II. EXPERIMENTAL DETAILS

Single crystals of Li_2O were grown, using a floating zone method[9] on sintered powder rods prepared from 99.5% pure lithium oxide grains furnished by Cerac Inc. A spectrometric analysis of one crystal gave as main impurities (in at. ppm) 34.0 Mg, 29.0 Al, 18.4 Na, 3.3 Si, 0.9 Fe, 0.7 Cu, 0.4 K. The obtained cylindrical bars were 80-mm long and with an average diameter of 5 mm. Two crystals had been grown in this manner, which had served subsequently in different methods of sample preparation. The first, called X-1, was sliced without cutting fluid with a diamond blade saw, and the final samples were obtained by cleavage to yield typically $\lesssim$1-mm-thick transparent platelets oriented parallel to (111). The second, X-2, was cut by means of a tungsten wire saw, with SiC-powder suspension in glycerol as a medium, allowing better geometry control and, thus, thinner (down to 100 μm) platelets. As far as possible, the slices were kept under vacuum to prevent pollution by air moisture.

The electron irradiations were performed with a 2.5 MeV Van de Graaff accelerator. The samples were wrapped with a 10-μm-thick copper foil and suspended in hydrogen gas used as cooling fluid. The beam was perpendicular to a (111) plane. The electron energy was chosen to be 1 or 2.5 MeV ensuring uniform damage across the sample thickness [only 150 keV are lost by 1 MeV electrons in 0.5 mm Li_2O (Ref. 10)], and the irradiation current controlled such as to maintain the sample temperature at 275 ± 5 K: a typical value was 40 $\mu A/cm^2$.

EPR experiments were done with a Bruker ER 200D X-band spectrometer operating at 9.5 GHz, in the 4–300 K temperature range. A TE_{104} double cavity was used, with a $CuSO_4$ standard kept at room temperature, in order to correct for the possible cavity Q-factor variation with temperature.

Microwave dielectric constant measurements were done on the same specimens using a TE_{10n} cavity with eight useful resonant modes, connected in a transmission regime to an HP8510C network analyzer; the resonances are in the range 7–15 GHz. The measurement of the shift in frequency Δf and of the Q factor $\Delta(Q^{-1})$ permitted us to determine the real and imaginary parts of the dielectric constant $\epsilon=\epsilon'-i\epsilon''$. These measurements are only performed at room temperature.

A thermal annealing treatment was applied to some of the irradiated specimens by heating them in a dynamic vacuum in steps of 50 degrees, for one hour each, up to the disappearance of the introduced damage.

For electron-microscopic observations, irradiated single crystals of Li_2O were cleaved under argon atmosphere and a suitable edge region of a chip selected. Polycrystalline specimens were crushed to powder and deposited between two copper grids in order to minimize charging of this highly insulating material. The observations were performed on a 300-kV Philips CM30. The electron energy was varied between 200 and 300 keV in the hope of determining a threshold for defect formation. The sample holder was mounted on a cold finger which permits stable measurements down to 100 K, thus limiting the mobility and agglomeration of eventually created color centers under the microscope beam. Optical microscopy was performed using a binocular Olympus SZH microscope provided with a Polaroid camera and a polarizing Reichert Polyvar transmission microscope with digital photography.

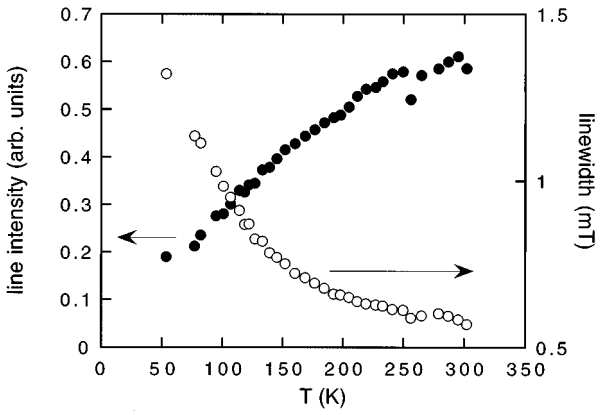

FIG. 1. ●: temperature variation of the broad EPR line intensity obtained by double integration of the Dysonian fit, for a sample irradiated with 8.7×10^{19} e^-/cm^2. ○: temperature variation of the width of the broad EPR line.

III. EPR RESULTS

Our study on polycrystals[4] established that room-temperature electron irradiation was required in order to get metal colloid creation. Therefore, all the samples described hereafter were irradiated at 275 ± 5 K.

A. EPR line

As described in Ref. 8, a typical EPR signal detected in an electron-irradiated sample clearly decomposes in two lines: a very narrow one (peak-to-peak width around 10^{-2} mT), Lorentzian in shape, whose saturation properties are compatible with a $T_1\approx T_2$ behavior and a broader line, not saturated with full microwave power (250 mW). The latter exhibits closely the ''metallic'' shape described by Feher and Kip after a model by Dyson,[11] taking the classical value 2.55 for the lobe height ratio A/B. It follows from the numerical fit that the two lines are centered at $g=2.0023$. It is worth recalling that in our work on polycrystals,[4] we observed only one single symmetric and narrow line corresponding to the narrower line; no broad line was detected.

Figure 1 shows the variation with temperature of the intensity of the broad line, in a sample irradiated with a fluence of 8.7×10^{19} e^-/cm^2 (13.9 C/cm^2). This figure can be compared with Fig. 2 of Ref. 8, for another sample. On both figures, the variation of the broad line intensity with temperature is unusual: it *increases*, a fact which we shall interpret below. The narrow line intensity follows a Pauli law, i.e., is temperature independent from helium to room temperature.

Figure 1 gives also the variation with temperature of the width of the broad line, in the same sample. The width given here is extracted from the Dysonian fit and corresponds to the $1/\gamma T_2$ value. In the same temperature range, the narrow line width decreases from 25 μT at 4 K to 13 μT at 300 K.

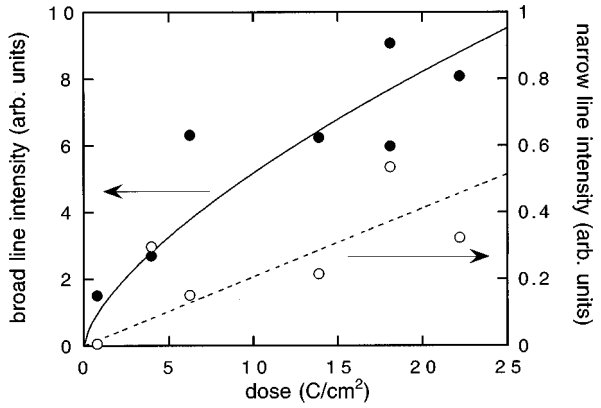

FIG. 2. ●: dose variation of the broad EPR line intensity at 300 K; ○: dose variation of the narrow EPR line intensity. The data are given in the same arbitrary units.

B. Variation with irradiation dose

We give in Fig. 2 the variation with irradiation dose of the intensities of the two lines, for crystals irradiated with 1 MeV electrons. Even if the points are quite dispersed, there is a clear tendency that intensity increases with dose; for the narrow line the law is not far from linear, whereas for the broad one, some kind of saturation seems to appear. This saturation will be discussed below.

In Fig. 3 for the same samples, the variation with dose of the widths of the two lines is given. The broad line width decreases with dose, whereas there is no clear cut variation of the narrow line width.

C. Annealing behavior

We have annealed a few irradiated crystals till the disappearance of the EPR signals. During the annealing process the sample color, black after irradiation, becomes gray and then more or less white. When the highest temperatures are reached, the samples seem to loose their cohesion and fall into pieces: there is no complete recovery to the preirradiated state.

We give in Fig. 4 the variation of the two line intensities with isochronal annealing temperature. There is a striking difference between the behaviors of these two lines: the narrow one disappears below 300 °C while the broad one first

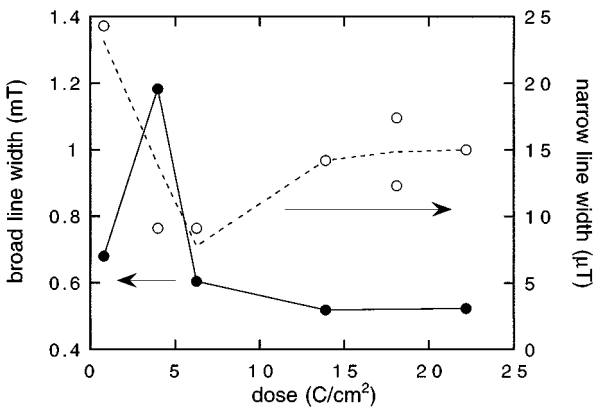

FIG. 3. Dose variation of the EPR line widths at 300 K: ●—broad line; ○—narrow line.

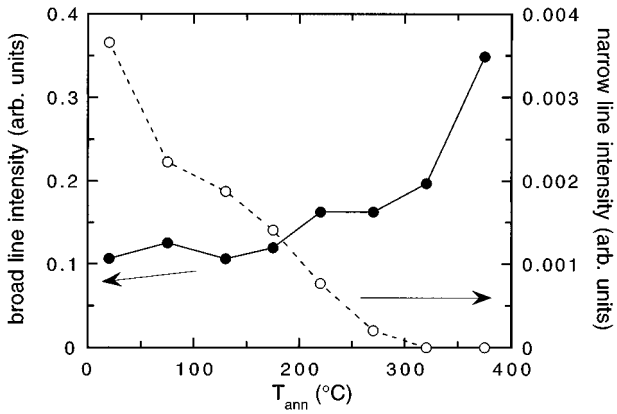

FIG. 4. Isochronal annealing behavior of the EPR line intensities in a Li_2O crystal irradiated with 3.9×10^{19} e^-/cm^2; the EPR spectra are taken at room temperature. The initial intensities correspond to radiation-induced spin concentrations of 2.48×10^{-3}, for the broad line, and 1.05×10^{-4}, for the narrow one: ●—broad line; ○—narrow line. The data are given in the same arbitrary units.

increases in intensity before disappearing only near 400 °C when the crystal decomposes. In Fig. 5 the variation with annealing temperature of the two line widths is represented. The width of the broad line clearly increases under annealing, while that of the narrow shows only a slightly growing tendency. A low-temperature EPR experiment after the 320 °C anneal revealed the same characteristics of the broad line as before annealing.

D. Discussion

All the above presented EPR results enable us to confirm unambiguously that the two lines correspond to two kinds of metallic lithium colloids.

(i) The narrow EPR line, with its free-electron g value and even more its Pauli-like T dependence, stems from metallic lithium. The Lorentzian line shape proves that these Li colloids are quite small, with a radius lower than the skin depth δ at 9 GHz, which is around $1\,\mu$m for a typical metal. These colloids correspond to those we observed in polycrystaline Li_2O samples irradiated near room temperature.[4] This is corroborated by the annealing behavior of the narrow line, which is the same for single and polycrystals.

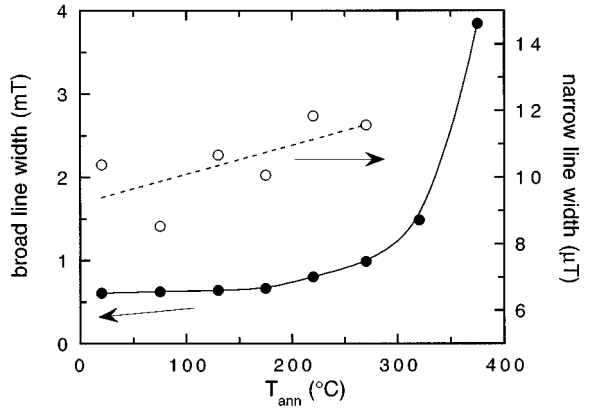

FIG. 5. Isochronal annealing behavior of the EPR line widths: ●—broad line; ○—narrow line.

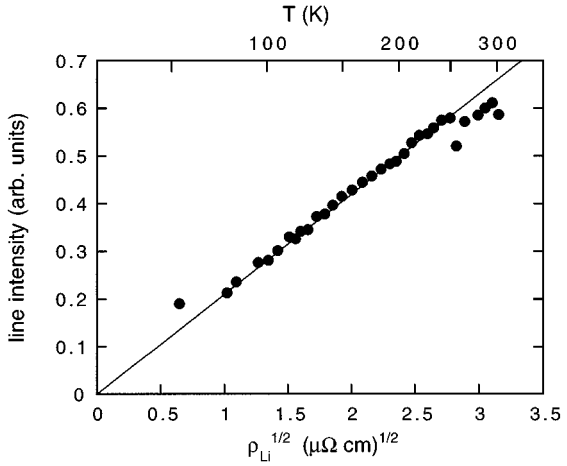

FIG. 6. Broad EPR line intensity plotted versus the square root of the bulk metallic Li resistivity $\sqrt{\rho}$. The straight line shows the good observance of the proportionality law. The upper scale gives the temperature.

(ii) The broader EPR line is of a Dysonian shape[11] through the whole measured temperature range; its g value and its T dependence, very far from a Curie law, strongly suggest that it corresponds also to metallic lithium. Such asymmetric shapes, caused by mixing absorption and dispersion responses, imply that this second kind of colloids is much larger than $1\,\mu$m.

As to the unusual temperature dependence of the line intensity for the broad line, it is related to the fact that the skin depth δ decreases when T decreases, so that only a surface layer of each colloid is observed. In the classical treatment of the Dysonian line shape, the signal intensity is proportional to δ, thus to the square root of the metal resistivity. The strongly varying intensity implies that the resistivity must remain highly T dependent, in a manner comparable to bulk lithium. Figure 6 checks that point: we plotted signal intensity versus the square root of Li resistivity, as given by Pifer and Magno.[12] The linear law is very satisfactorily obeyed, confirming the idea that the intensity variation is due to skin depth penetration. Under these conditions, it is very likely that, as noted in Ref. 8, an integration of the EPR line underestimates the spin concentration corresponding to the asymmetric line.

In a preceding paper[8] we gave a discussion on the relevant relaxation times and characteristic lengths in our large colloids. Calling T_D the electronic diffusion time through δ, T_2 the spin relaxation time, and δ_e the spin-free path, we got $\delta \approx 1.6\ \mu$m and $\delta_e \approx 10\ \mu$m at room temperature: according to Ref. 12, this is not compatible with the $A/B = 2.55$ Dysonian regime, for which $\delta_e < \delta$ and $\delta_e < r$. This implies much smaller values of δ_e, yielding much greater values for the colloidal metal resistivity compared to that of bulk lithium. This, in turn, could possibly mean that the structure of our large Li colloids is not the same as that of bulk metallic Li.

Another interesting result is the increase of the broad line intensity during annealing (Fig. 4). One first possible interpretation is an agglomeration of the small colloids leading to an increased large-colloid population. However, as the total volume of large colloids is typically 30 times larger than that of the small ones, this possibility seems unlikely. The eventual increase, for some unknown reason, of metallic resistivity during annealing, giving rise to a corresponding increase of skin depth, is another possible interpretation.

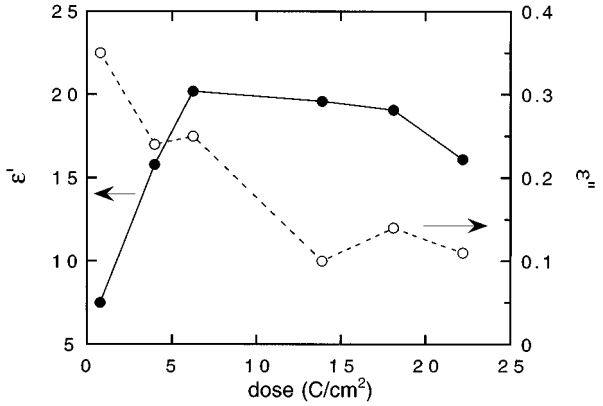

FIG. 7. Real and imaginary parts of the dielectric constant ϵ' (●) and ϵ'' (○), taken at 9 GHz and 300 K, versus irradiation dose.

Finally, we come back to the discussion of Figure 2: while the line intensity due to small colloids follows the natural (for small concentrations) proportionality law versus dose, the intensity corresponding to the large colloids is well described, considering the data dispersion, by a $d^{2/3}$ law, where d is the irradiation dose. Such a law is indeed expected if the volume of produced metal increases linearly with dose, as only the surface of each colloid is reached by the EPR experiment.

IV. DIELECTRIC CONSTANT RESULTS

Unirradiated lithium oxide possesses $\epsilon' \approx 6$ and $\epsilon'' \approx 0.00(1)$ in our frequency range. This has to be compared with the values of the real and imaginary parts of the dielectric constant after irradiation with various electron doses: these are given in Fig. 7, where one can see the very substantial effect of irradiation both on the real part as well as on the imaginary part of ϵ. This effect anneals as shown in Fig. 8. One curious observation, reproducible for the two samples studied, is the strong peak in ϵ'' centered at 400 °C, just before the complete recovery of ϵ, while there is no particular effect on ϵ'. The ϵ'' increase is, in fact, much larger than the initial radiation induced $\Delta\epsilon''_{\rm irr}$ and its beginning seems to coincide with the complete recovery of the narrow line. We have also to mention that ϵ' is roughly constant between 7 and 15 GHz, while ϵ'' is proportional to the frequency f.

We attribute the increase of both components of ϵ under irradiation to the formation of metallic colloids. First, as discussed in Ref. 4 for polycrystals, this increase appears only for $T_{\rm irr} \geqslant 200$ K, which is precisely the minimum temperature for colloid creation. Samples irradiated at lower temperature or by γ rays, which contain only color centers (F^+ centers) give no ϵ enhancement. Second, the recovery temperature for ϵ corresponds to the disappearing of colloids as seen by EPR. Last, this recovery temperature is higher for single crystals, in which large colloids exist, than for polycrystals[4] where only small colloids can be formed, recovering at lower $T_{\rm ann}$.

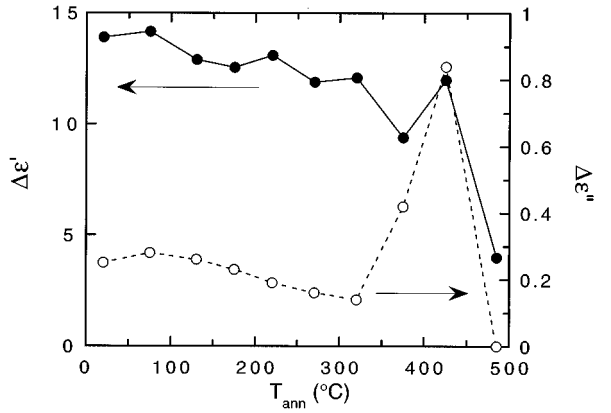

FIG. 8. Annealing behavior of the radiation-induced changes of the dielectric constant $\Delta\epsilon'$ (●) and $\Delta\epsilon''$ (○) taken at 9 GHz and 300 K. Note the strong peaking of $\Delta\epsilon''$ after anneals near 400 °C just before recovery.

Let us now invoke the classical models for describing the dielectric constant of mixtures of two components. The archetype of such a mixing law is the so-called Maxwell Garnett model,[13] based on the Clausius-Mossotti approximation, which describes the specimen as an assembly of dielectric spheres embedded in an insulating matrix; other models can be cited, such as that by Bruggeman,[13] but for very low metallic concentrations like ours (in the range 10^{-3} to 10^{-2} typically), there is no significant difference. The Maxwell Garnett formula is

$$\frac{\epsilon-\epsilon_h}{\epsilon+2\epsilon_h}=x\frac{\epsilon_i-\epsilon_h}{\epsilon_i+2\epsilon_h}, \tag{1}$$

where ϵ is the relative dielectric constant of the sample, ϵ_i that of inclusions, and ϵ_h that of the host; x is the volume fraction of the inclusions. For the metallic case one can use, in mks units,

$$\epsilon_i''=\frac{\sigma}{\epsilon_0\omega}\gg 1, \tag{2}$$

for $\rho_{Li}=10\,\mu\Omega$ cm and $f=10$ GHz, this gives $\epsilon_i''=1.8\times10^7$. For such values, and considering that $x\ll1$, it follows that

$$\epsilon'=\epsilon_h(1+3x), \tag{3}$$

$$\epsilon''=\frac{\epsilon_h^2}{\epsilon_i'}\,9x. \tag{4}$$

The result of such a trial is unambiguous: it is not possible to account for our significant variations of both ϵ' and ϵ'' with such models. The only way to get rid of this paradox is to consider nonisotropic models, generalizing for instance the Maxwell Garnett model by using ellipsoids instead of spheres. Calling n the depolarizing factor[14] of the ellipsoid (all the ellipsoids are supposed to have the same orientation), we get

$$\frac{\epsilon-\epsilon_h}{\epsilon_h+n(\epsilon-\epsilon_h)}=x\frac{\epsilon_i-\epsilon_h}{\epsilon_h+n(\epsilon_i-\epsilon_h)}. \tag{5}$$

This expression reduces to Eq. (1) for the spheric case for which $n=1/3$. We get for $x\ll1$

$$\epsilon'=\epsilon_h\left(1+\frac{x}{n}\right), \tag{6}$$

$$\epsilon''=\frac{\epsilon_h^2}{\epsilon_i''}\,\frac{x}{n^2}. \tag{7}$$

The ϵ' and ϵ'' values may become substantial if n becomes small, that is in a needle or disk geometry. We thus tentatively attribute to such an anisotropy of our colloids the significant variation of ϵ displayed in Fig. 7. We notice that Eq. (7) gives a natural explanation for the proportionality between ϵ'' and the frequency, through the variation of ϵ_i'' [Eq. (2)]. However, things are not yet very clear: first we need, for fitting our experimental results, $n\sim x$, which corresponds to *very* thin needles or flat disks; second, the anisotropic Maxwell Garnett model described here is oversimplified, as in reality the orientations of the different ellipsoids are surely more or less randomly distributed. This last fact could be one source of the difference of the ϵ'' values between single and polycrystals. It could also play a role in the ϵ'' peak revealed on the recovery curve in Fig. 8. One might wonder if this effect is related to a redistribution or an additional production of metallic lithium stemming from the sample decomposition, which begins in this range, as signaled in Sec. IIIC.

In Fig. 7, after an initial increase, ϵ' seems to saturate whereas ϵ'' decreases. In the simple model given above, this would be compatible with n increasing linearly with x, i.e., metallic disks of constant number and diameter, increasing in thickness.

V. MICROSCOPY

A. Electron microscopy

We have investigated both polycrystalline Li_2O crushed to powder and crystal chips obtained by cleavage, after Li-colloid introduction through bombardment with high-energy electrons. Generally, the samples were in steady evolution under a microscope voltage of 300 kV, clearly indicating defect creation with such a beam energy. On the other hand, they were quite stable and permitted reasonable observation with a voltage of 200 kV; at 250 kV, long-term work was no longer feasible and one had to change the observed area frequently. Thus, we suggest a value of $E_d=(250^{+10}_{-25})$ keV as threshold energy for defect formation by the impinging electrons. Since it was shown in Ref. 4 that the primary defects created in Li_2O by an electron irradiation were F^+ centers, i.e., oxygen vacancies, it is reasonable to relate the above threshold energy to a threshold for displacing an oxygen atom from its regular site. The corresponding transmitted atomic displacement energy $T_d(\mathrm{eV})=(560.8/A)(E_d/m_ec^2)(2+E_d/m_ec^2)$, with A as the atomic mass and $m_ec^2=511$ keV, is then $T_d^{\mathrm{O}}=(43^{+2}_{-5})$ eV. This is a rather satisfactory value when compared to the closely related system MgO, with a similar damage mechanism, where Pells[15] had determined a $T_d^{\mathrm{O}}=53$ eV.

Having established stable experimental conditions at 200 kV (at a temperature of 100 K) we have tried to observe any additional structures within the regular Li_2O lattice which

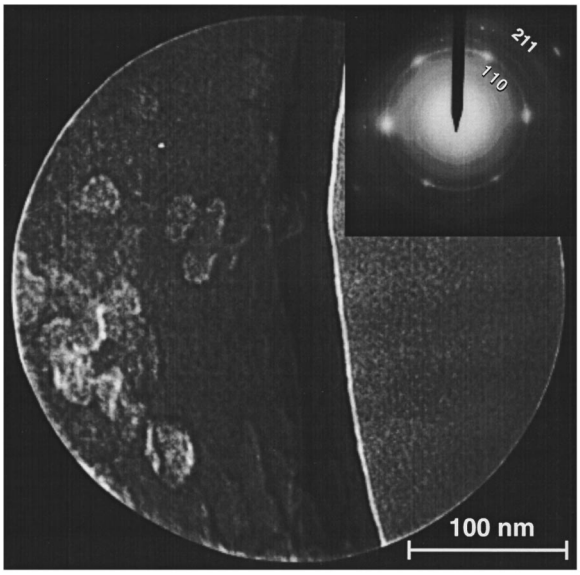

FIG. 9. Electron microscope bright field image of a chip edge of an irradiated (by 1 MeV electrons) Li_2O crystal, taken at 200 kV and at $T=100$ K, exhibiting Li colloids. Inset: diffraction image of a region overlapping a colloid platelet. Note the diffuse rings superimposed upon the narrow Li_2O pattern and attributed to Li nanocrystals.

could be possibly attributed to metalic lithium colloids. A typical example is presented in Fig. 9, which shows a chip edge of a freshly cleaved Li_2O crystal containing oval platelets of $100-200$ Å size compatible with the analysis of the dielectric constant in the preceding section. A diffraction pattern of this region (shown in the inset) exhibits, besides the spots and the narrow rings due to Li_2O, two rather irregular diffuse rings characteristic for diffracting nanocrystals of various sizes.[16] These rings cannot be attributed to possibly present LiOH or Li_2CO_3; they can, however, be indexed as (110) and (211) respectively within a simple cubic or a bcc lattice, with a parameter $a'=2.84$ Å. (For a reminder, the lattice constant of bulk bcc lithium metal is $a_0=3.51$ Å.) It is tempting to assign these reflections to lithium nanocrystals formed out of the simple cubic Li unit occupying the tetrahedral sites of the Li_2O cell. In fact, the parameter a' of this new, larger, unit cell seems to be related to the parameter $a/2$ of the original Li sublattice ($a=4.61$ Å is the lattice constant of Li_2O), such that $a'\approx(3/2)^{1/2}a/2$, which could mean that the face diagonal of the former coincides with the space diagonal of the latter. Furthermore, a bcc unit cell of parameter a' yields roughly the same atomic volume per Li atom as the simple cubic cell with parameter $a/2$, certainly a favorable condition for colloid growth.

B. Optical microscopy

After having found possible candidates for the small Li colloids in the above described electron microscope investigations, we were looking for the larger ($>1\mu$m) structures using optical microscopy. The specimens containing metallic colloids were usually black and opaque, thus enabling, in general, only surface investigations in reflection. A few relatively thin chips bombarded with 2.5 MeV electrons were, however, sufficiently transparent to permit transmission experiments. It is here (Fig. 10) that we have noted the surprising structures briefly mentioned in our recent paper.[8]

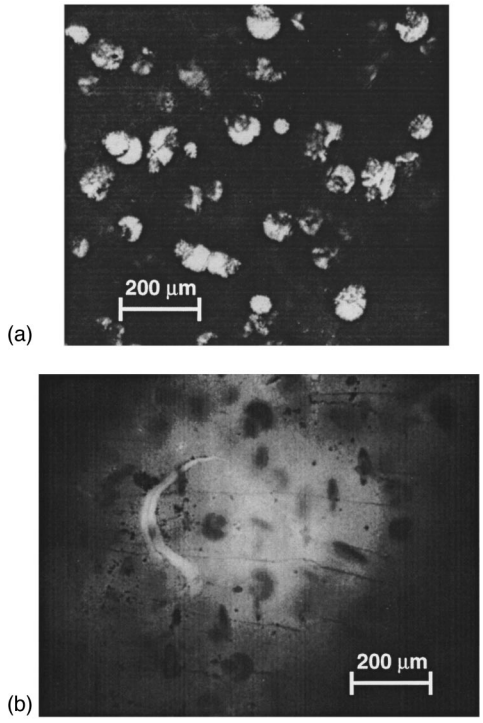

FIG. 10. Optical microscope image of an irradiated (by 2.5 MeV electrons) Li_2O crystal chip parallel to (111), in reflection (a) and in transmission (b) exhibiting metallic Li colloids (spheres and ''mushrooms'') and possibly oxygen filled {100} oriented cavities (''cigars''). The sickle shape in (b) is a surface scratch.

The reflection image [Fig. 10(a)] exhibits brilliant, metallically shining spherical objects of $20-25$ μm in diameter, which sometimes agglomerate to yield (more or less complex) mushroomlike configurations. In transmission [Fig. 10(b)], we see, first, that these ''mushrooms'' are apparently distributed randomly across the whole crystal thickness and, second, we note the presence of oval, cigarlike shapes not visible in reflection. Contrarily to the ''mushrooms,'' the ''cigars'' seem to be oriented preferentially, namely in three directions at an angle of about 60° to each other. Knowing that the chip surface is a (111) cleavage plane we can try to assign them to the three {100} projections upon it.

As to the origin of these structures, it seems obvious to attribute the metalliclike spheres and mushrooms to the looked for earlier identified large lithium colloids (see Sec. III), while the cigarlike shades could be cavities aligned through internal stress along (100)—either empty or filled with oxygen gas. The latter suggestion is probably more appealing as it would be an indication for the final fate of the displaced oxygen atoms. Alternatively, the observed structures could be disclike configurations oriented along the four planes of the {111} family: one parallel to the surface and the other three inclined to it. Only the former would be capable of reflecting incident light.

VI. CONCLUSION

We have shown that one can create a significant concentration of lithium metal colloids by electron-irradiating single

crystals of lithium oxide near room temperature.

(i) The two EPR metallic lines observed correspond to two kinds of colloids: the very narrow Lorentzian line comes from small colloids (size $<1\mu$m), whereas the broader one, of Dysonian shape, is associated with much larger colloids (size $\gg 1\mu$m). An analysis of the EPR properties of these large colloids seems to indicate that the spin-free path is much lower than in bulk Li. In an annealing treatment, the two types of colloids disappear at clearly distinct temperatures, corroborating the qualitative difference between them.

(ii) Dielectric constant measurements in the microwave frequency range after irradiation and anneal confirm the metallic character of the colloids. In addition, their analysis in the framework of the Maxwell Garnett model suggests a strong shape anisotropy, which is also observed by electron microscopy.

(iii) Optical microscopy permits us to detect large colloids of typically 20-μm size, which appear oriented along preferential lattice directions.

ACKNOWLEDGMENTS

We wish to thank A. Revcolevschi for advice in crystal growth and A. Barbu and L. Reining for useful discussions. This work was supported in part by the European Fusion Technology Program, Task No. UT-M-CM1.

*Electronic address: francois.beuneu@polytechnique.fr

†Electronic address: peter.vajda@polytechnique.fr

[1] A.E. Hughes and S.C. Jain, Adv. Phys. **28**, 717 (1979).

[2] F. Beuneu and P. Monod, Phys. Rev. B **18**, 2422 (1978); P. Monod and F. Beuneu, *ibid.* **19**, 911 (1979).

[3] S. Albrecht, G. Onida, and L. Reining, Phys. Rev. B (to be published).

[4] P. Vajda and F. Beuneu, Phys. Rev. B **53**, 5335 (1996).

[5] M. Lambert, Ch. Mazières, and A. Guinier, J. Phys. Chem. Solids **18**, 129 (1961); C. Taupin, *ibid.* **28**, 41 (1967).

[6] K. Noda, K. Uchida, T. Tanifuji, and S. Nasu, Phys. Rev. B **24**, 3736 (1981); K. Noda, Y. Ishii, H. Matsui, and H. Watanabe, Radiat. Eff. **97**, 297 (1986); for a more complete list, see Ref. 4.

[7] P. Vajda and F. Beuneu, *REI*-8, *VIII International Conference on Radiation Effects in Insulators, Catania*, Italy, 1995 [Nucl. Instrum. Methods Phys. Res. B **116**, 183 (1996)].

[8] F. Beuneu and P. Vajda, Phys. Rev. Lett. **76**, 4544 (1996).

[9] J. Shindo, S. Kimura, K. Noda, T. Kurasawa, and S. Nasu, J. Nucl. Mater. **79**, 418 (1979).

[10] L. Pagès, E. Bertel, H. Joffre, and L. Sklavenitis, Commissariat á l'Energie Atomique, Report No. CEA-R-3942 (1970).

[11] G. Feher and F. Kip, Phys. Rev. **98**, 337 (1955); F.J. Dyson, *ibid.* **98**, 349 (1955).

[12] J.H. Pifer and R. Magno, Phys. Rev. B **3**, 663 (1971).

[13] R. Landauer, in *Electrical Transport and Optical Properties of Inhomogeneous Media*, edited by J.C. Garland and D.B. Tanner, AIP Conf. Proc. No. 40 (AIP, New York, 1978), p. 2.

[14] J.A. Osborn, Phys. Rev. **67**, 351 (1945).

[15] G.P. Pells, Radiat. Eff. **64**, 71 (1982).

[16] For a recent review, see, for example, *Proceedings of the International Conference on Electron Microscopy*, ICEM 13-Paris, 1994, edited by B. Jouffrey and C. Colliex (Editions de Physique, Paris, 1994), and references therein.